

RESEARCH LETTER

10.1002/2017GL076315

Key Points:

- KHI in the subsolar region is critically important for boundary layer dynamics in Jupiter's magnetosphere
- Simulations show that duskward moving KH waves originate at around 10 MLT, and stationary KH waves form on the dawnside around 08–09 MLT
- Duskside density fluctuations associated with KHI exhibit much longer periodicity compared to those on the dawnside

Correspondence to:

B. Zhang,
binzheng@ucar.edu

Citation:

Zhang, B., Delamere, P. A., Ma, X., Burkholder, B., Wiltberger, M., Lyon, J. G., ... Sorathia, K. A. (2018). Asymmetric Kelvin-Helmholtz instability at Jupiter's magnetopause boundary: Implications for corotation-dominated systems. *Geophysical Research Letters*, 45, 56–63. <https://doi.org/10.1002/2017GL076315>








Received 14 NOV 2017

Accepted 18 DEC 2017

Accepted article online 22 DEC 2017

Published online 8 JAN 2018

Asymmetric Kelvin-Helmholtz Instability at Jupiter's Magnetopause Boundary: Implications for Corotation-Dominated Systems

B. Zhang^{1,2} , P. A. Delamere³, X. Ma⁴ , B. Burkholder³ , M. Wiltberger¹ , J. G. Lyon⁵ , V. G. Merkin⁶ , and K. A. Sorathia⁶ 

¹High Altitude Observatory, National Center for Atmospheric Research, Boulder, CO, USA, ²Department of Earth Sciences, University of Hong Kong, Hong Kong, ³Geophysical Institute, University of Alaska Fairbanks, Fairbanks, AK, USA, ⁴Physical Science Department, Embry-Riddle Aeronautical University, Daytona Beach, FL, USA, ⁵Department of Physics and Astronomy, Dartmouth College, Hanover, NH, USA, ⁶Applied Physics Laboratory, The Johns Hopkins University, Laurel, MD, USA

Abstract The multifluid Lyon-Fedder-Mobarry (MFLFM) global magnetosphere model is used to study the interactions between solar wind and rapidly rotating, internally driven Jupiter magnetosphere. The MFLFM model is the first global simulation of Jupiter magnetosphere that captures the Kelvin-Helmholtz instability (KHI) in the critically important subsolar region. Observations indicate that Kelvin-Helmholtz vortices are found predominantly in the dusk sector. Our simulations explain that this distribution is driven by the growth of KHI modes in the prenoon and subsolar region (e.g., >10 local time) that are advected by magnetospheric flows to the dusk sector. The period of density fluctuations at the dusk terminator flank (18 magnetic local time, MLT) is roughly 1.4 h compared with 7.2 h at the dawn flank (6 MLT). Although the simulations are only performed using parameters of the Jupiter's magnetosphere, the results may also have implications for solar wind-magnetosphere interactions at other corotation-dominated systems such as Saturn. For instance, the simulated average azimuthal speed of magnetosheath flows exhibit significant dawn-dusk asymmetry, consistent with recent observations at Saturn. The results are particularly relevant for the ongoing Juno mission and the analysis of dawnside magnetopause boundary crossings for other planetary missions.

1. Introduction

Magnetic local time asymmetries are ubiquitous in planetary magnetospheres. Dawn-dusk asymmetries are particularly evident in the rapidly rotating giant magnetospheres; the solar wind interaction must, fundamentally, play an important role (Hill et al., 1983; Khurana, 2001). There has been considerable debate regarding the nature of the solar wind interaction with the giant planet magnetospheres. Following the observations of Jupiter's magnetotail from 150 R_J to >2500 R_J made by the New Horizons spacecraft in the spring of 2007, there has been considerable debate regarding the role of the solar wind in the dynamics of Jupiter's magnetosphere (Cowley et al., 2008; McComas & Bagenal, 2007, 2008). Much of the subsequent debate is summarized by Delamere (2015) and compares the relative importance of large-scale reconnection (Dungey, 1961), a viscous-like interaction (Axford & Hines, 1961), with the internally driven Vasyliunas cycle (Vasyliunas, 1983). Delamere and Bagenal (2010, 2013) argued that a viscous-like interaction, generating tangential drag, may play a dominant role in the solar wind interaction due to the large sheared flows (maximum on the dawn flank and minimum on the dusk flank) that exist on the dayside magnetopause boundaries. A consequence of large flow shears is a Kelvin-Helmholtz (KH) unstable magnetopause boundary.

Nonlinear KH waves can efficiently transport momentum, plasma, and energy as either a large-scale diffusion process (e.g., Ma et al., 2017; Miura, 1984), or a small-scale turbulent process (e.g., Nakamura et al., 2017). For a two-dimensional geometry, theoretical analysis (Miura, 1984), numerical magnetohydrodynamics (MHD) simulations (Nykyri & Otto, 2001, 2004), and hybrid simulations (Cowee et al., 2009, 2010) showed that the transport rate of the Kelvin-Helmholtz instability (KHI) (i.e., diffusion coefficient) is close to the canonical diffusivity required to populate the low-latitude boundary layer (Sonnerup, 1980). Delamere et al. (2011) demonstrated that the diffusion coefficient due to 2-D KH plasma mixing is expected to be more than

$1 \times 10^{10} \text{ m}^2/\text{s}$ at Saturn's magnetopause, which can play a significant role in driving magnetospheric dynamics. Recently, Ma et al. (2017) used a 3-D MHD simulation to show that the diffusion coefficient caused by a 3-D nonlinear KH wave is 1 order of magnitude higher than a 2-D nonlinear KH wave. The faster-growing KH mode leads to a higher diffusion coefficient, which consequently forms a wider boundary.

There is abundant evidence that the KHI is active at Saturn's magnetopause boundary (Delamere et al., 2013; Masters et al., 2009, 2010, 2012; Wilson et al., 2012). An initially surprising result was evidence for more KH activity in the postnoon sector where the sheared flow is minimized (i.e., magnetodisc corotation and sheath flows are both tailward). However, Ma et al. (2015), using a two-dimensional (2-D) MHD simulation of Saturn's dayside magnetopause, showed that KH vortices originating in the subsolar region (roughly from 11 to 14 local times) are transported to the postnoon sector and the wavelength is enlarged due to the gradient of sheared flow. To validate the simulation results, Ma et al. (2015) conducted a comprehensive boundary normal analysis (minimum variance analysis, MVA) of Cassini data and found that indeed the boundary normal directions fluctuate in a systematic manner consistent with the 2-D simulation results. Meanwhile, KH vortices formed in the prenoon sector (<10 MLT) tend to diffuse rapidly and form a boundary layer, precluding the existence of well-defined vortex structures. As a result, vortex structures are more likely to be observed in the postnoon sector. Recently, Burkholder et al. (2017) showed a significant dawn-dusk flow asymmetry in Saturn's magnetosheath. The dawnside flows in the vicinity of the magnetopause boundary were reduced by roughly 75 km/s with respect to the expected asymptotic flank value of 200 km/s (Desroche et al., 2013). Burkholder et al. (2017) argued that tangential drag generated by small-scale and intermittent reconnection associated with the KH instability can account for the flow reduction (Ma et al., 2017).

In this paper, we present results from the multifluid Lyon-Fedder-Mobarry (MFLFM) global magnetosphere model of corotation-dominated magnetospheres using Jupiter as an example. The results are particularly relevant for the ongoing Juno mission and the analysis of dawnside magnetopause boundary crossings (e.g., Gershman et al. (2017)). This is the first global simulation of the giant magnetospheres that captures the local time asymmetry of the KH instability including the development of vortices in the subsolar region. Previous models (e.g., Fukazawa et al., 2007; Walker et al., 2011) capture KH activity on the dawn and dusk flanks but not in the critically important subsolar region. The results may also have implications for other corotation-dominated magnetospheres such as Saturn; therefore, qualitative comparisons with observations at Saturn are also discussed.

2. Simulation Information

The global Jupiter magnetosphere model is adapted from the multifluid version of the Lyon-Fedder-Mobarry (MFLFM) global magnetosphere model, which has been used extensively to study the solar wind-magnetosphere interactions (e.g., Brambles et al., 2010, 2011; Wiltberger et al., 2010). The basic finite volume (FV) numerical methods of solving the ideal magnetohydrodynamics (MHD) equations are described in Lyon et al. (2004). The multifluid version of the code, which builds on the same numerical techniques used in the single fluid LFM, allows each ion species to move under its own force balance. The FV techniques enables calculations on a nonorthogonal, curvilinear grid adapted to the Jupiter magnetospheric boundary layer simulations; that is, the grid cells are approximately aligned with the shape of the Jupiter magnetopause with cells smaller across the nominal bow shock than parallel to it. The computational kernel of the LFM code uses an eighth-order spatial reconstruction scheme together with the Partial Donor Cell limiter (Hain, 1987) such that the code maintains nonoscillatory solutions with minimum amount of numerical diffusion. Combined with the adapted grid, the MFLFM schemes can resolve a shear layer near the magnetopause boundary within two or three cells, which is suitable for KHI simulations with moderate grid resolution. The magnetic reconnection in the MFLFM code is controlled by the conditions external to the reconnection zone through the conservation of mass, momentum, and magnetic flux. The rate of reconnection is constrained by a Petschek-like inflow condition to be a fraction (≈ 0.1) of the Alfvén speed in the inflow. Details about the properties of magnetic reconnection in the code can be found in Ouellette et al. (2014) and in the supporting information of Zhang et al. (2017).

For the simulations of Jupiter's magnetosphere, the stretched spherical grid extends 100 Jupiter radii (R_J) in the sunward direction, $-1000 R_J$ in the antisunward direction, and $\pm 300 R_J$ in the directions perpendicular to the Sun-Jupiter axis. The highest grid resolution for the MFLFM model is used for the Jupiter simulations. The grid resolution is nonuniform, with $0.2 R_J$ near the magnetopause and approximately $0.25 R_J$ near the

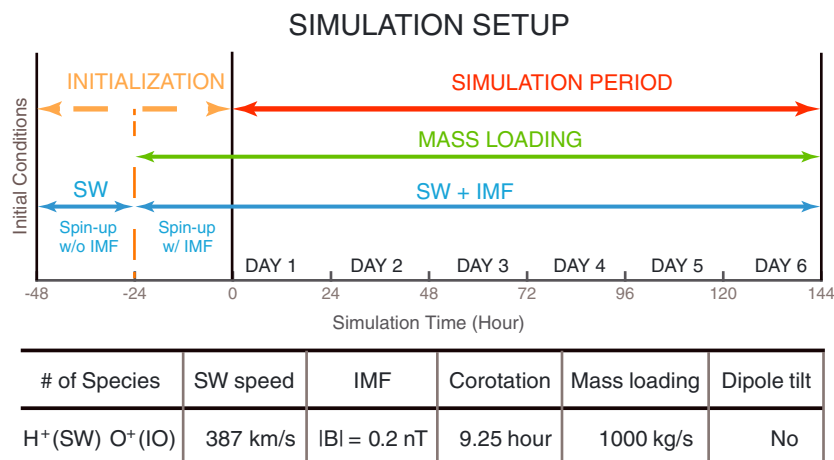


Figure 1. The time history of the test simulations and a summary of the simulation setups.

inner region. The low-altitude computational boundary is set to be at $6 R_J$ where the orbit of Io is in order to simplify the implementation of mass loading from Io.

The test simulations were performed using two ion species, namely, H⁺ from upstream solar wind (SW) and O⁺ from Io. The 1,000 kg/s mass loading from Io is introduced at the equator of the inner boundary. The mass loading module performs an extra step after the hydrodynamic update but before the Lorentz force and magnetic field updates (Varney et al., 2016). The extra O⁺ mass fluxes, momentum fluxes, and energy fluxes through the inner interface are calculated from the mass loading parameters, and the active cells adjacent to the inner interface are updated according to these extra fluxes. This procedure ensures that the rate at which plasma enters Jupiter’s magnetosphere exactly equals the rate at which it is specified using the Io parameters without creating numerical mass loading through the MHD solver.

The simulations were driven by idealized solar wind (SW) and interplanetary magnetic field (IMF) conditions. The time history of the driving conditions and other simulation setups are summarized in Figure 1. Three test simulations were performed, driven by northward ($B_z = +0.2$ nT), southward ($B_z = -0.2$ nT), and westward ($B_y = +0.2$ nT) IMF with the same magnitude, respectively. In each simulation, after the rotating magnetosphere was preconditioned by upstream, supersonic H⁺ solar wind for 24 h, both O⁺ mass loading with a fixed rate of 1,000 kg/s and IMF condition were introduced for another 24 h. After the 48 h precondition, the test simulations were run for another 144 h (six Earth days) driven by the corresponding IMF orientations. The IMF B_x component were set to 0 and the SW $V_x = -378$ km/s, $V_y = V_z = 0$. The upstream SW fluid has a number density of 0.2 cm^{-3} and a sound speed of 30 km/s, respectively. These solar wind parameters are consistent with the average solar wind dynamic pressure at Jupiter (Jackman & Arridge, 2011). The dipole tilt angle of the Jupiter magnetosphere was set to 0 in order to remove hemispheric asymmetries and simplify the analysis. The 9.25 h corotation of the Jupiter magnetosphere is implemented through imposing a time-stationary corotation potential to the ionospheric potential, which is a function of magnetic latitude.

3. Simulation Results

Figures 2a–2c show the instantaneous distributions of H⁺ number density in the equatorial plane derived from the three test simulations driven by the same solar wind conditions with different IMF orientations: $B_z = +0.2$ nT, $B_z = -0.2$ nT, and $B_y = +0.2$ nT, respectively. The simulation time for the snapshots of equatorial H⁺ density is 18:00 simulation time (ST). The number density of H⁺ in the simulated Jupiter inner magnetosphere is relatively small during the whole simulation period (less than 0.1 cm^{-3}) regardless of the orientation of the upstream IMF, suggesting that the solar wind entry is less sensitive to the orientation of the driving IMF. In other words, the effect of the Dungey cycle is not evident in the idealized Jupiter magnetosphere simulations, especially for the $B_z = +0.2$ nT case in which dayside reconnection is enabled efficiently (Jupiter’s dipole moment is in the opposite direction compared to the Earth). However, the average locations of the bow shock in the simulations shown in Figures 2a and 2b are approximately $2 R_J$ sunward compared to the simulation driven by $B_z = 0.2$ nT (Figure 2c), which is approximately 3% change, suggesting that the IMF orientation does

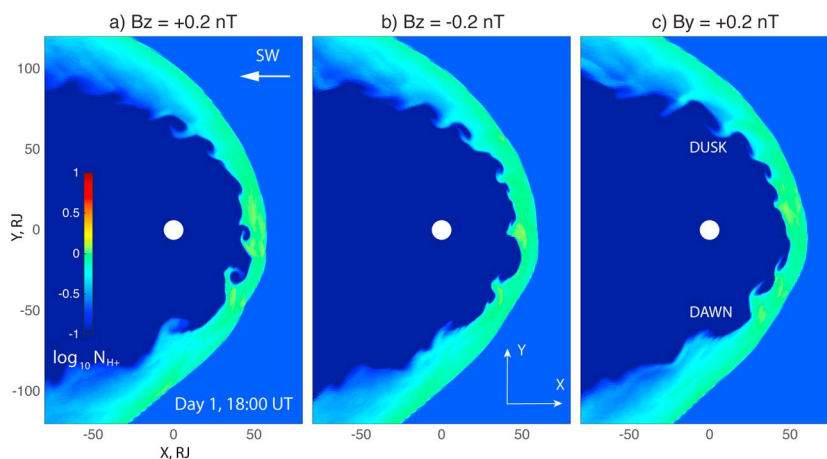


Figure 2. Instantaneous distributions of KH instability in the equatorial plane driven by (a) $B_z = +0.2$ nT, (b) $B_z = -0.2$ nT, and (c) $B_y = +0.2$ nT. The snapshots are taken at 18:00 ST in each test simulation.

affect the interaction between solar wind and the Jupiter's magnetosphere. Note that the simulated magnetopause boundary is dynamic at all local time sectors due to the presence of KH activity. The 144 h averaged subsolar magnetopause locations calculated from the three simulations are approximately 47.5, 48.6, and 48.8 R_J , suggesting that the effects of IMF orientation on the location of Jupiter's magnetopause are relatively small compared to the Earth's magnetosphere due, in part, to the internal plasma pressure that contributes to the magnetopause location.

The simulated shape of Jupiter's magnetosheath is asymmetric in the equatorial plane due to the fast corotation of Jupiter's magnetosphere. In the test simulation driven by IMF B_y , the average bow shock location at the y axis is $-105.5 R_J$ on the dawnside and $+100.4 R_J$ on the duskside. The magnetopause boundary is quite dynamic but also asymmetric in an average sense. In the simulation driven by IMF B_z , the 144 h averaged magnetopause location (through tracing the last closed magnetic field lines using average simulated magnetic fields) is not adequate for capturing nonadiabatic heating processes known to occur within Jupiter's magnetodisc (Bagenal & Delamere, 2011). This difference will be investigated in future studies, and this paper focuses on the interaction between the solar wind and Jupiter's magnetosphere rather than nonideal internal processes.

The Kelvin-Helmholtz vortices along the magnetopause boundary are evident in the spatial distributions of the simulated magnetosheath density throughout the whole simulation. As an example, Figures 2a–2c show snapshots from the three test simulations driven by different IMF orientations at 18:00 ST. It is found that in the three simulations with $|B| = 0.2$ nT, both the evolution and spatial extension of the KH vortices at the magnetopause are not sensitive to the IMF orientations, possibly due to the fact that the simulated Jupiter's magnetosheath is hydrodynamically dominated rather than magnetohydrodynamically dominated (with sheath plasma $\beta \gg 1$). Thus, KHI may be triggered at high latitudes away from the equatorial plane (e.g., Hwang et al., 2012). The dawn-dusk asymmetry in the spatial distribution of the KH vortices is evident in each simulation. It is clear that the spatial extension of the KH vortices is smaller along the duskside magnetopause compared to those on the dawnside magnetopause regardless of the orientation of the IMF, suggesting that the influence of magnetic tension force on the growth rate of KHI is relatively small. This is consistent with the results by Desroche et al. (2012, 2013). At the Earth's magnetopause, global MHD simulations have shown that the large-scale vortices move along the magnetopause without significant dawn-dusk asymmetries in spatial extensions during pure northward IMF (Guo et al., 2010; Merkin et al., 2013). The temporal evolution of the KH vortices also exhibits significant dawn-dusk asymmetry as shown in Figure 3b. As an example, in the test simulation between 18:00 and 19:40 ST, KH vortices are generated in the subsolar region between 10 and 12 MLT and then advected toward the duskside. Previous global simulations capture the KH vortices on the dawn/dusk flank region but not the subsolar sector, which is critically important for the generation of dawn-dusk asymmetry in the distribution of KH vortices along the magnetopause. Between 18:00 and 19:40 ST, the vortices travel at an average azimuthal speed around 237 km/s on the duskside, with spatial separations approximately 10–20 R_J in the postnoon sector. On the dawnside, the traveling speed of the vortices

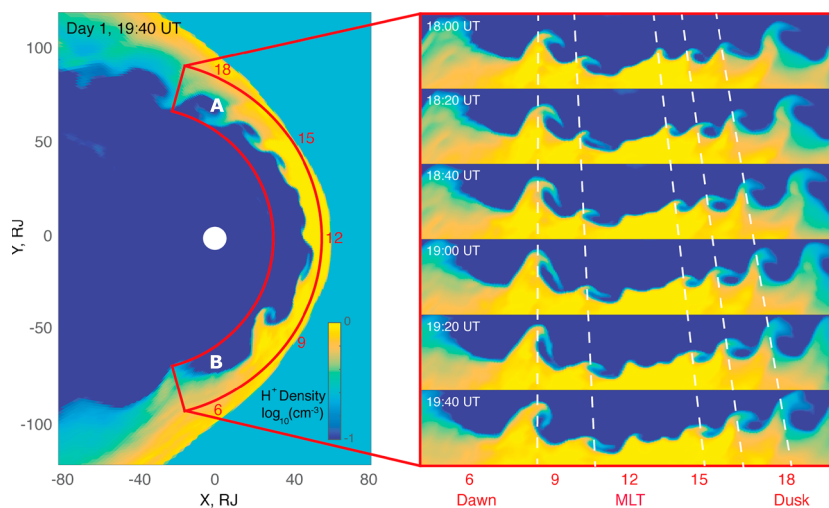


Figure 3. The KH instability: (left) a snapshot of H^+ number density in the equatorial plane at 19:40 ST; (right) temporal evolution of the KH vortices between 18:00 and 19:40 ST.

is much lower than that on the duskside, suggesting that the simulated KH structure is almost stagnant on magnetopause boundary in the morning sector between 7 and 10 MLT. The reason for the stagnant structure on the dawnside is mainly the fast rotation of the Jupiter magnetosphere. On the dawnside, the magnetosheath velocity is antiparallel to the rotation of the magnetospheric flow. Thus, the large shear flow is satisfied with the KH unstable condition (Chandrasekhar, 1961). However, the net tangential (i.e., perpendicular to the boundary normal direction) momentum is relatively small on the dawnside, leading to stationary vortices because the KH wave propagates at a speed of

$$v_{\text{KHI}} = \frac{\rho_M v_M + \rho_S v_S}{\rho_M + \rho_S}, \quad (1)$$

where ρ_M and v_M are defined as the magnetospheric total mass density and bulk flow velocity, while ρ_S and v_S are defined as the magnetosheath density and velocity, respectively. It is also interesting to note that Masters et al. (2010) observed a long-lived (few hours) KH vortex at 10 LT, which is consistent with our simulation result. In the simulated evolution of KHI shown in Figure 3, the contribution of magnetospheric O^+ to the total mass density near the magnetopause is essentially 0 compared to H^+ . Future studies with much longer simulation periods and mass loading rates are needed to investigate possible influences of internal processes associated with the transport of O^+ on the boundary layer dynamics at Jupiter's magnetopause.

The dawn-dusk asymmetry is also evident in the temporal variations of plasma density near the magnetopause boundary layer. Figure 4 shows the simulated plasma density on the duskside and dawnside as a

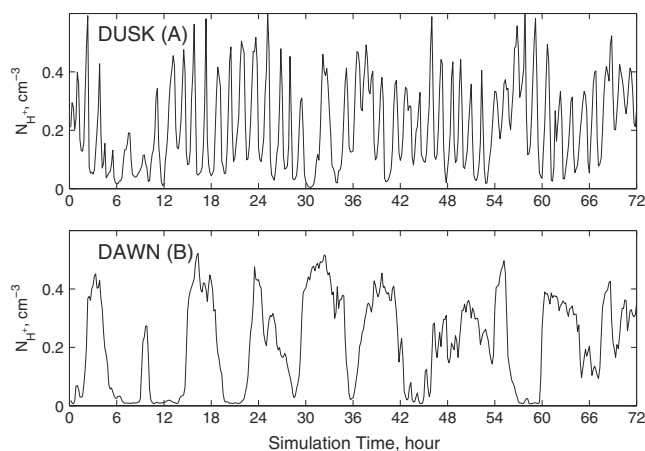


Figure 4. Time series of H^+ number density taken from the dusk and dawn flanks (points A and B in Figure 3, respectively).

function of time, respectively, derived from the test simulation driven by IMF B_y . Similar results were also found in the other two test simulations driven by IMF B_z (not shown). The time series of the duskside density shown in Figure 4 is recorded at $(0, 66 R_J)$ on the equatorial plane (indicated as point "A" in Figure 3, left), and the dawnside density variation shown in Figure 4a is recorded at $(0, -66 R_J)$ on the equatorial plane (indicated as point "B" in Figure 3, left). On the duskside, the temporal variation of plasma number density has a period of approximately 1.4 h, while on the dawnside, the corresponding period in the plasma density variation is around 7.2 h, which is a consequence of the simulated dawn-dusk asymmetry in the spatial extension and the azimuthal speed of the KH vortices. This simulated dawn-dusk asymmetry in the density structures of the KH vortices is qualitatively consistent with in situ Cassini data analyses (Ma et al., 2015).

The simulated flow speed within Jupiter's magnetosheath also exhibits significant dawn-dusk asymmetry. Figure 5a shows the average azimuthal magnetosheath flow speed (v_ϕ) in the equatorial plane calculated from

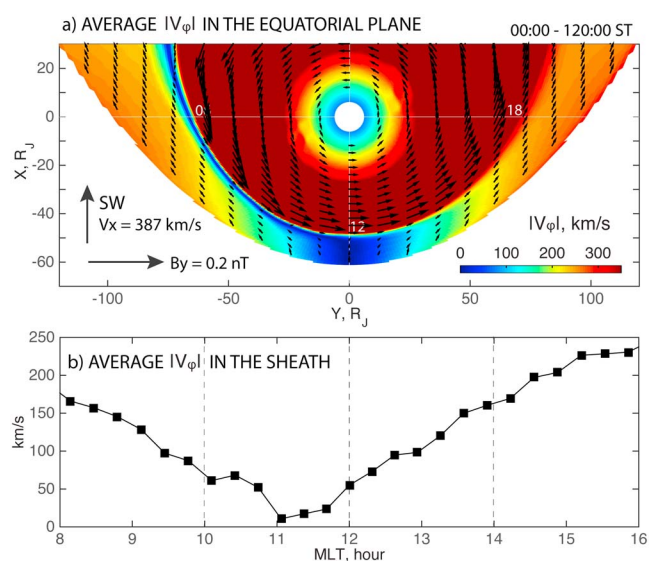


Figure 5. The local time asymmetry of the azimuthal component (v_ϕ) of sheath flows.

the test simulation driven by IMF B_y . It is evident that magnetic local time asymmetry is also seen in the average shape of the magnetopause boundary. Near the magnetopause boundary on the dawnside (06–12 MLT), the magnitude of average v_ϕ in the magnetosheath is less than 100 km/s, while near the duskside magnetopause boundary (12–18 MLT), the magnitude of average v_ϕ in the magnetosheath is greater than 150 km/s. Figure 5b shows the corresponding MLT distribution of average magnetosheath flow speed v_ϕ calculated within the magnetosheath. The average v_ϕ in the prenoon sector (10–12 MLT) is approximately 41 km/s, while the average v_ϕ in the postnoon sector (12–14 MLT) is approximately 106 km/s. Although the numerical experiments are developed based on parameters of Jupiter's magnetosphere, the asymmetric distribution of magnetosheath flow is in qualitative agreement with recent observed flow asymmetry in Saturn's magnetosheath (Burkholder et al., 2017). Future analysis is needed to quantify, in detail, the stresses leading to tangential drag at the magnetopause boundary, and future observational studies are needed to verify the simulated asymmetric flow speeds in Jupiter's magnetosheath.

4. Summary and Discussion

Using the multifluid Lyon-Fedder-Mobarry model, we have conducted the first global simulation of the giant planet magnetospheres that captures the

observed dawn-dusk asymmetries associated with the growth and evolution of Kelvin-Helmholtz vortices on the magnetopause boundary. The growth of KH modes in the subsolar region is critical for understanding the prevalence of KH vortices found along the dusk flank where flow shears are minimized and in some cases may render the magnetopause boundary *stable*. Magnetospheric (sub)corotational flows advect these vortices through the subsolar region and into the dusk sector. The temporal signature of density variations on the dusk terminator flank has a much shorter period (1.4 h) compared with the dawn flank (7.2 h). Interestingly, 1.4 h is similar to the 60 to 70 min quasi periodicity (QP-60) found in multiple instruments predominantly in Saturn's dusk sector magnetodisc (Palmaerts et al., 2016; Roussos et al., 2016). It remains unclear whether these modulations are associated with KH vortices directly or whether KH modes may be responsible for exciting magnetospheric eigenoscillations (Glassmeier, 1995). Evidence of a shorter period (QP-15 and QP-40) at Jupiter might suggest the latter (see review by Delamere, 2016).

We have also performed simulations driven by the same SW/IMF with grid resolutions that are twice as coarse in each direction compared to the grid resolution used in the above sections. In the lower-resolution simulations, although the growth rate of KHI is lower, the simulated dawn-dusk asymmetry and the local time extensions of KHI vortices along the magnetopause remain approximately the same. In future studies we will investigate the sensitivity of model results to grid resolutions that are higher than the current resolution used in this study, analyze stresses and transport at the magnetopause boundary, explore the effect of varying solar wind parameters, and provide a detailed analysis of the internal plasma and magnetic flux transport to understand the role of the solar wind interaction for the giant, internally driven magnetospheres. The results of such studies will be particularly relevant for the ongoing Juno mission at Jupiter as well as the analysis of Cassini data at Saturn.

References

- Axford, W. I., & Hines, C. O. (1961). A unifying theory of high latitude geophysical phenomena and geomagnetic storms. *Canadian Journal of Physics*, 39, 1433–1464. <https://doi.org/10.1139/p61-172>
- Bagenal, F., & Delamere, P. A. (2011). Flow of mass and energy in the magnetospheres of Jupiter and Saturn. *Journal of Geophysical Research*, 116, A05209. <https://doi.org/10.1029/2010JA016294>
- Brambles, O. J., Lotko, W., Damiano, P. A., Zhang, B., Wiltberger, M., & Lyon, J. (2010). Effects of causally driven cusp O^+ outflow on the storm time magnetosphere-ionosphere system using a multifluid global simulation. *Journal of Geophysical Research*, 115, A00J04. <https://doi.org/10.1029/2010JA015469>
- Brambles, O. J., Lotko, W., Zhang, B., Wiltberger, M., Lyon, J., & Strangeway, R. J. (2011). Magnetosphere sawtooth oscillations induced by ionospheric outflow. *Science*, 332(6034), 1183–1186. <https://doi.org/10.1126/science.1202869>
- Burkholder, B., Delamere, P. A., Ma, X., Thomsen, M. F., Wilson, R. J., & Bagenal, F. (2017). Local time asymmetry of Saturn's magnetosheath flows. *Geophysical Research Letters*, 44, 5877–5883. <https://doi.org/10.1002/2017GL073031>
- Chandrasekhar, S. (1961). *Hydrodynamic and hydromagnetic stability*. New York: Oxford University Press.

Acknowledgments

The research was supported by the National Center for Atmospheric Research (NCAR). We would like to acknowledge high-performance computing support from Cheyenne (doi:10.5065/D6RX99HX) provided by NCAR's Computational and Information Systems Laboratory, sponsored by the National Science Foundation (NSF). Michael Wiltberger was serving at the NSF during the production of this paper. Any opinion, findings, conclusions, or recommendations expressed in this material are those of the authors and do not necessarily reflect the views of the NSF. Simulation data, simulation codes, and analysis routines are being preserved on the NCAR High Performance Storage System and will be made available upon written request to the lead author.

- Cowee, M. M., Winske, D., & Gary, S. P. (2009). Two-dimensional hybrid simulations of superdiffusion at the magnetopause driven by Kelvin-Helmholtz instability. *Journal of Geophysical Research*, *114*, A10209. <https://doi.org/10.1029/2009JA014222>
- Cowee, M. M., Winske, D., & Gary, S. P. (2010). Hybrid simulations of plasma transport by Kelvin-Helmholtz instability at the magnetopause: Density variations and magnetic shear. *Journal of Geophysical Research*, *115*, A06214. <https://doi.org/10.1029/2009JA015011>
- Cowley, S. W. H., Badman, S. V., Imber, S. M., & Milan, S. E. (2008). Comment on "Jupiter: A fundamentally different magnetospheric interaction with the solar wind" by D. J. McComas and F. Bagenal. *Geophysical Research Letters*, *35*, L10101. <https://doi.org/10.1029/2007GL032645>
- Delamere, P. A. (2015). Solar wind interaction with giant magnetospheres and Earth's magnetosphere. In A. Keiling, C. M. Jackman, & P. A. Delamere (Eds.), *Magnetotails in the Solar System*. Hoboken, NJ: John Wiley & Sons. <https://doi.org/10.1002/9781118842324>
- Delamere, P. A. (2016). *A review of the low-frequency waves in the giant magnetospheres*, *Geophysical Monograph Series* (Vol. 216, pp. 365–378). Washington, DC: American Geophysical Union. <https://doi.org/10.1002/9781119055006.ch21>
- Delamere, P. A., & Bagenal, F. (2010). Solar wind interaction with Jupiter's magnetosphere. *Journal of Geophysical Research*, *115*, A10201. <https://doi.org/10.1029/2010JA015347>
- Delamere, P. A., & Bagenal, F. (2013). Magnetotail structure of the giant magnetospheres: Implications of the viscous interaction with the solar wind. *Journal of Geophysical Research: Space Physics*, *118*, 7045–7053. <https://doi.org/10.1002/2013JA019179>
- Delamere, P. A., Wilson, R. J., & Masters, A. (2011). Kelvin-Helmholtz instability at Saturn's magnetopause: Hybrid simulations. *Journal of Geophysical Research*, *116*, A10222. <https://doi.org/10.1029/2011JA016724>
- Delamere, P. A., Wilson, R. J., Eriksson, S., & Bagenal, F. (2013). Magnetic signatures of Kelvin-Helmholtz vortices on Saturn's magnetopause: Global survey. *Journal of Geophysical Research: Space Physics*, *118*, 393–404. <https://doi.org/10.1029/2012JA018197>
- Desroche, M., Bagenal, F., Delamere, P. A., & Erkaev, N. (2012). Conditions at the expanded Jovian magnetopause and implications for the solar wind interaction. *Journal of Geophysical Research*, *117*, A07202. <https://doi.org/10.1029/2012JA017621>
- Desroche, M., Bagenal, F., Delamere, P. A., & Erkaev, N. (2013). Conditions at the magnetopause of Saturn and implications for the solar wind interaction. *Journal of Geophysical Research: Space Physics*, *118*, 3087–3095. <https://doi.org/10.1002/jgra.50294>
- Dungey, J. W. (1961). Interplanetary magnetic field and the auroral zones. *Physical Review Letters*, *6*(2), 47–48. <https://doi.org/10.1103/PhysRevLett.6.47>
- Fukazawa, K., Ogino, T., & Walker, R. J. (2007). Vortex-associated reconnection for northward IMF in the Kronian magnetosphere. *Geophysical Research Letters*, *34*, L23201. <https://doi.org/10.1029/2007GL031784>
- Gershman, D. J., DiBraccio, G. A., Connerney, J. E. P., Hospodarsky, G., Kurth, W. S., Ebert, R. W., ... Bolton, S. J. (2017). Juno observations of large-scale compressions of Jupiter's dawnside magnetopause. *Geophysical Research Letters*, *44*, 7559–7568. <https://doi.org/10.1002/2017GL073132>
- Glassmeier, K.-H. (1995). Ultralow-frequency pulsations: Earth and Jupiter compared. *Advances in Space Research*, *16*, 209–218. [https://doi.org/10.1016/0273-1177\(95\)00232-4](https://doi.org/10.1016/0273-1177(95)00232-4)
- Guo, X. C., Wang, C., & Hu, Y. Q. (2010). Global MHD simulation of the Kelvin-Helmholtz instability at the magnetopause for northward interplanetary magnetic field. *Journal of Geophysical Research*, *115*, A10218. <https://doi.org/10.1029/2009JA015193>
- Hain, K. H. (1987). The partial donor cell method. *Journal of Computational Physics*, *73*(1), 131–147. [https://doi.org/10.1016/0021-9991\(87\)90110-0](https://doi.org/10.1016/0021-9991(87)90110-0)
- Hill, T. W., Dessler, A. J., & Goertz, C. K. (1983). Magnetospheric Models. In A. J. Dessler (Ed.), *Physics of the Jovian magnetosphere* (pp. 353–394). Cambridge, UK: Cambridge University Press.
- Hwang, K.-J., Goldstein, M. L., Kuznetsova, M. M., Wang, Y., Viñas, A. F., & Sibeck, D. G. (2012). The first in situ observation of Kelvin-Helmholtz waves at high-latitude magnetopause during strongly dawnward interplanetary magnetic field conditions. *Journal of Geophysical Research*, *117*, A08233. <https://doi.org/10.1029/2011JA017256>
- Jackman, C. M., & Arridge, C. S. (2011). Solar cycle effects on the dynamics of Jupiter's and Saturn's magnetospheres. *Solar Physics*, *274*, 481–502. <https://doi.org/10.1007/s11207-011-9748-z>
- Khurana, K. K. (2001). Influence of solar wind on Jupiter's magnetosphere deduced from currents in the equatorial plane. *Journal of Geophysical Research*, *106*, 25,999–26,016. <https://doi.org/10.1029/2000JA000352>
- Lyon, J. G., Fedder, J. A., & Mobarrry, C. M. (2004). The Lyon-Fedder-Mobarrry (LFM) global MHD magnetospheric simulation code. *Journal of Atmospheric and Solar-Terrestrial Physics*, *66*, 1333–1350. <https://doi.org/10.1016/j.jastp.2004.03.020>
- Ma, X., Stauffer, B., Delamere, P. A., & Otto, A. (2015). Asymmetric Kelvin-Helmholtz propagation at Saturn's dayside magnetopause. *Journal of Geophysical Research: Space Physics*, *120*, 1867–1875. <https://doi.org/10.1002/2014JA020746>
- Ma, X., Delamere, P., Otto, A., & Burkholder, B. (2017). Plasma transport driven by the three-dimensional Kelvin-Helmholtz instability. *Journal of Geophysical Research: Space Physics*, *122*, 10,382–10,395. <https://doi.org/10.1002/2017JA024394>
- Masters, A., Achilleos, N., Bertucci, C., Dougherty, M. K., Kanani, S. J., Arridge, C. S., ... Coates, A. J. (2009). Surface waves on Saturn's dawn flank magnetopause driven by the Kelvin-Helmholtz instability. *Planetary and Space Science*, *57*, 1769–1778. <https://doi.org/10.1016/j.pss.2009.02.010>
- Masters, A., Achilleos, N., Cutler, J., Coates, A., Dougherty, M., & Jones, G. (2012). Surface waves on Saturn's magnetopause. *Planetary and Space Science*, *65*(1), 109–121. <https://doi.org/10.1016/j.pss.2012.02.007>
- Masters, A., Achilleos, N., Kiverson, M. G., Sergis, N., Dougherty, M. K., Thomsen, M. F., ... Coates, A. J. (2010). Cassini observations of a Kelvin-Helmholtz vortex in Saturn's outer magnetosphere. *Journal of Geophysical Research*, *115*, A07225. <https://doi.org/10.1029/2010JA015351>
- McComas, D. J., & Bagenal, F. (2007). Jupiter: A fundamentally different magnetospheric interaction with the solar wind. *Geophysical Research Letters*, *34*, L20106. <https://doi.org/10.1029/2007GL031078>
- McComas, D. J., & Bagenal, F. (2008). Reply to comment by S. W. H. Cowley et al. on "Jupiter: A fundamentally different magnetospheric interaction with the solar wind". *Geophysical Research Letters*, *35*, L10103. <https://doi.org/10.1029/2008GL034351>
- Merkin, V. G., Lyon, J. G., & Claudepierre, S. G. (2013). Kelvin-Helmholtz instability of the magnetospheric boundary in a three-dimensional global MHD simulation during northward IMF conditions. *Journal of Geophysical Research: Space Physics*, *118*, 5478–5496. <https://doi.org/10.1002/jgra.50520>
- Miura, A. (1984). Anomalous transport by magnetohydrodynamic Kelvin-Helmholtz instabilities in the solar wind-magnetosphere interaction. *Journal of Geophysical Research*, *89*, 801–818. <https://doi.org/10.1029/JA089iA02p00801>
- Nakamura, T. K. M., Hasegawa, H., Daughton, W., Eriksson, S., Li, W. Y., & Nakamura, R. (2017). Turbulent mass transfer caused by vortex induced reconnection in collisionless magnetospheric plasmas. *Nature Communication*, *8*(1), 1582. <https://doi.org/10.1038/s41467-017-01579-0>
- Nykyri, K., & Otto, A. (2001). Plasma transport at the magnetospheric boundary due to reconnection in Kelvin-Helmholtz vortices. *Geophysical Research Letters*, *28*, 3565–3568. <https://doi.org/10.1029/2001GL013239>

- Nykyri, K., & Otto, A. (2004). Influence of the Hall term on KH instability and reconnection inside KH vortices. *Annales Geophysicae*, *22*, 935–949. <https://doi.org/10.5194/angeo-22-935-2004>
- Ouellette, J. E., Lyon, J. G., & Rogers, B. N. (2014). A study of asymmetric reconnection scaling in the Lyon-Fedder-Mobarry code. *Journal of Geophysical Research: Space Physics*, *119*, 1673–1682. <https://doi.org/10.1002/2013JA019366>
- Palmaerts, B., Roussos, E., Krupp, N., Kurth, W. S., Mitchell, D. G., & Yates, J. N. (2016). Statistical analysis and multi-instrument overview of the quasi-periodic 1-hour pulsations in Saturn's outer magnetosphere. *Icarus*, *271*, 1–18. <https://doi.org/10.1016/j.icarus.2016.01.025>
- Roussos, E., Krupp, N., Mitchell, D. G., Paranicas, C., Krimigis, S. M., Andriopoulou, M., ... Dougherty, M. K. (2016). Quasi-periodic injections of relativistic electrons in Saturn's outer magnetosphere. *Icarus*, *263*, 101–116. <https://doi.org/10.1016/j.icarus.2015.04.017>
- Sonnerup, B. U. O. (1980). Theory of the low-latitude boundary layer. *Journal of Geophysical Research*, *85*, 2017–2026. <https://doi.org/10.1029/JA085iA05p02017>
- Varney, R. H., Wiltberger, M., Zhang, B., Lotko, W., & Lyon, J. (2016). Influence of ion outflow in coupled geospace simulations: 1. Physics-based ion outflow model development and sensitivity study. *Journal of Geophysical Research: Space Physics*, *121*, 9671–9687. <https://doi.org/10.1002/2016JA022777>
- Vasyliunas, V. M. (1983). Plasma distribution and flow. In *Physics of the Jovian magnetosphere* (pp. 395–453). Cambridge, UK: Cambridge University Press.
- Walker, R. J., Fukazawa, K., Ogino, T., & Morozoff, D. (2011). A simulation study of Kelvin-Helmholtz waves at Saturn's magnetopause. *Journal of Geophysical Research*, *116*, A03203. <https://doi.org/10.1029/2010JA015905>
- Wilson, R. J., Delamere, P. A., Bagenal, F., & Masters, A. (2012). Kelvin-Helmholtz instability at Saturn's magnetopause: Cassini ion data analysis. *Journal of Geophysical Research*, *117*, A03212. <https://doi.org/10.1029/2011JA016723>
- Wiltberger, M., Lotko, W., Lyon, J. G., Damiano, P., & Merkin, V. (2010). Influence of cusp O⁺ outflow on magnetotail dynamics in a multifluid MHD model of the magnetosphere. *Journal of Geophysical Research*, *115*, A00J05. <https://doi.org/10.1029/2010JA015579>
- Zhang, B., Brambles, O. J., Cassak, P. A., Ouellette, J. E., Wiltberger, M., Lotko, W., & Lyon, J. G. (2017). Transition from global to local control of dayside reconnection from ionospheric-sourced mass loading. *Journal of Geophysical Research: Space Physics*, *122*, 9474–9488. <https://doi.org/10.1002/2016JA023646>